Supplementary Information for "Self-Formed Quantum Wires and Dots in GaAsP-GaAsP Core-Shell Nanowires"

H. Aruni Fonseka[1], Anton V. Velichko[2], Yunyan Zhang[3], James A. Gott[1], George D. Davis[2], Richard Beanland[1], Huiyun Liu[3], David J. Mowbray[2] and Ana M. Sanchez[1]**

[1]Department of Physics, University of Warwick, Coventry CV4 7AL, United Kingdom

[2] Department of Physics and Astronomy, University of Sheffield, Sheffield, S3 7RH, United Kingdom

[3] Department of Electronic and Electrical Engineering, University College London, London WC1E 7JE, United Kingdom

* Corresponding authors:

a.fonseka.1@warwick.ac.uk, a.m.sanchez@warwick.ac.uk

Section S1: Lateral cross-sectional TEM sample preparation process using microtome sectioning:

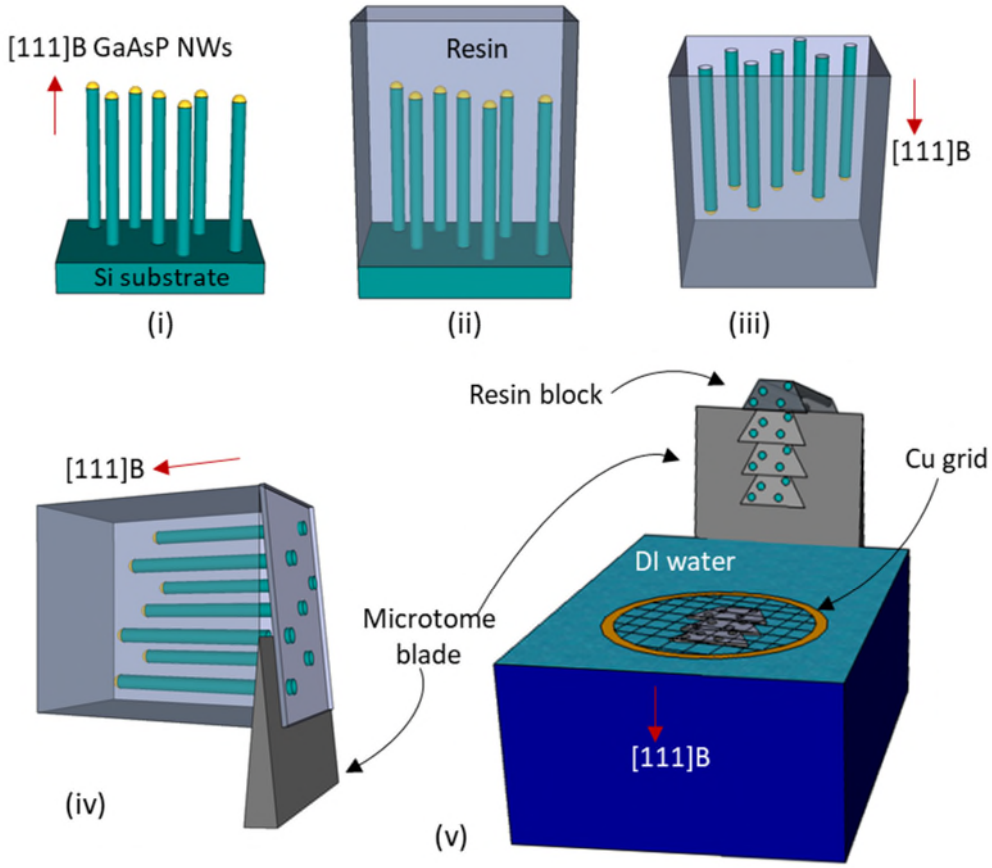

Figure S1. Process of cross-section sample preparation using a microtome, adapted from ref [1].

Usually, 200-400 nm from the base of the nanowires is lost during the substrate removal step (step (iii)). Thereafter, the sequence of slices progresses from the base to the tip of the nanowires. The direction of the sequence on the grids can be identified due to the trapezoidal shape of the slices. For the current sample, multiple, consecutive sets of sections were collected on separate grids due to the relatively long length of the nanowires.

Section S2: Polarity determination of the cross-sections

III-V nanowires commonly grow in the [111] B direction on Si (111) substrates. This has been shown to be true for GaAsP nanowires grown on Si (111)[2]. As indicated in Figure S1, the microtomed nanowire slices float-off in an orientation where the tip side, i.e. the [111] B direction is downwards. When collected on the TEM grid, the [111] B direction of the nanowires is directed upwards. The grids are inserted into the TEM so that the electron beam is incident on the sample side. This means that the [111] B direction is pointing upwards when inside the TEM.

Hence, the method elaborated in Jiang *et al.*[3] was used for the determination of the polarity of the <112> directions. This was further verified by atomic resolution images, as described in Zheng *et al.*[4], and shown in Figures S2 (c)-(e).

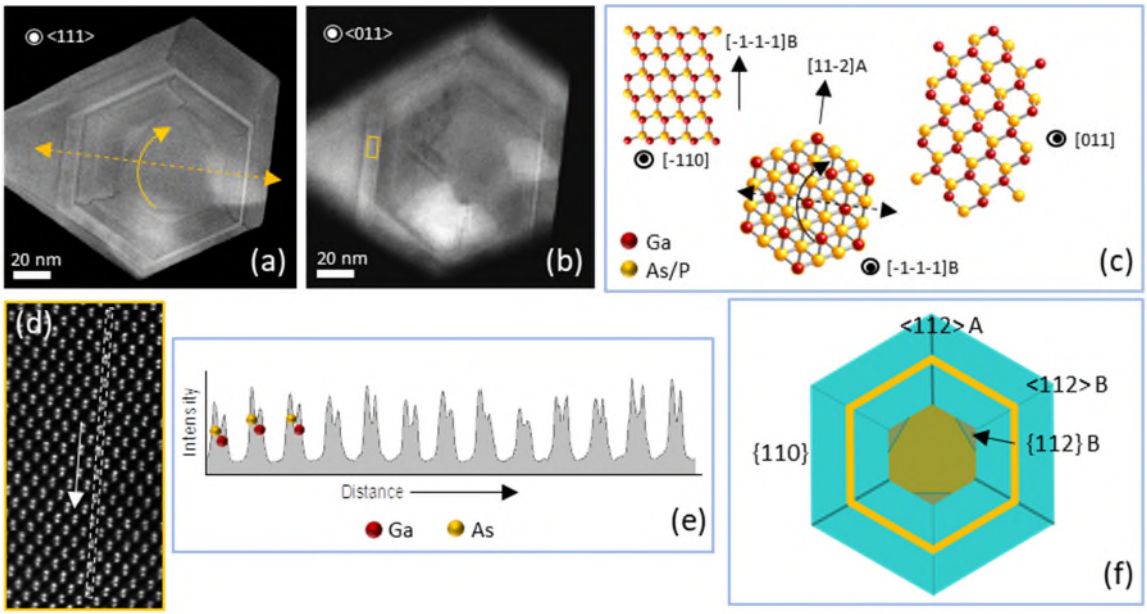

Figure S2. (a) Nanowire cross section shown in Figure 2 (b) of the main manuscript, viewed along <111> zone axis. The yellow curved arrow indicates the direction of tilt to reach <011> zone axis. (b) Same nanowire viewed along <011> zone axis, tilted ~35.3 ° from the position in (a). The yellow box indicates the area within the GaAs quantum well used for the atomic resolution image in (d). (c) Atomistic model of a slice from a nanowire, viewed along three different directions. The second and third models show the expected atom configurations for samples positions in (a) and (b), respectively. (d) Atomic resolution image from the area indicated in (b). (e) Intensity profile along the slice of atoms indicated by the dashed lines in (d), showing a configuration matching to that of the third model in (c). (f) Schematic showing the deduced polarities.

Section S3: Determination of the 3-dimensional form of the triangular regions using consecutive microtome sections

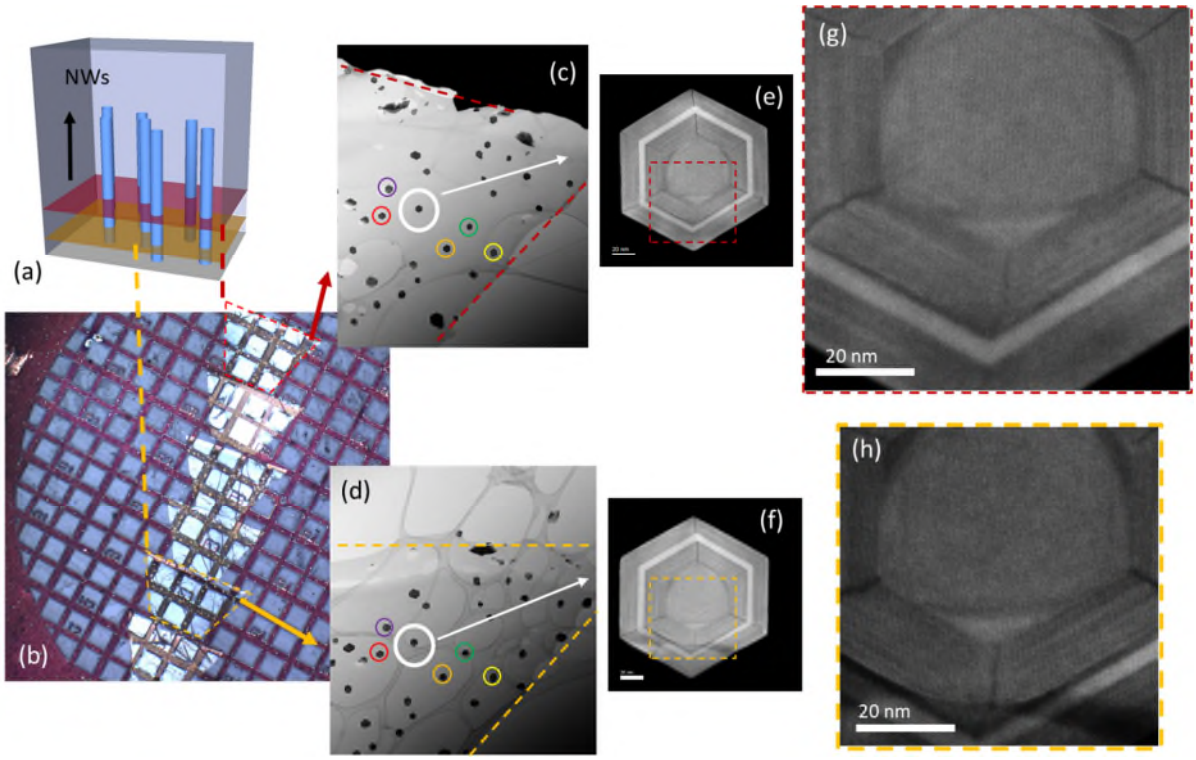

Figure S3. (a) Schematic showing consecutive slicing along the nanowire. (b) Optical microscope image of some consecutive slices picked up on a numbered TEM grid. Each slice is approximately 50 nm thick. (c) & (d) low magnification bright field STEM images from the corners of the slices marked in red and yellow, respectively. The respective coloured circles indicate the same nanowire in the two slices. (e) & (f) Higher magnification annular dark field (ADF) TEM images from the two slices of the nanowires indicated by the white circles. (g) & (h) Further magnified ADF TEM images of the triangular regions seen in (e) and (f).

Section S4: Strain maps

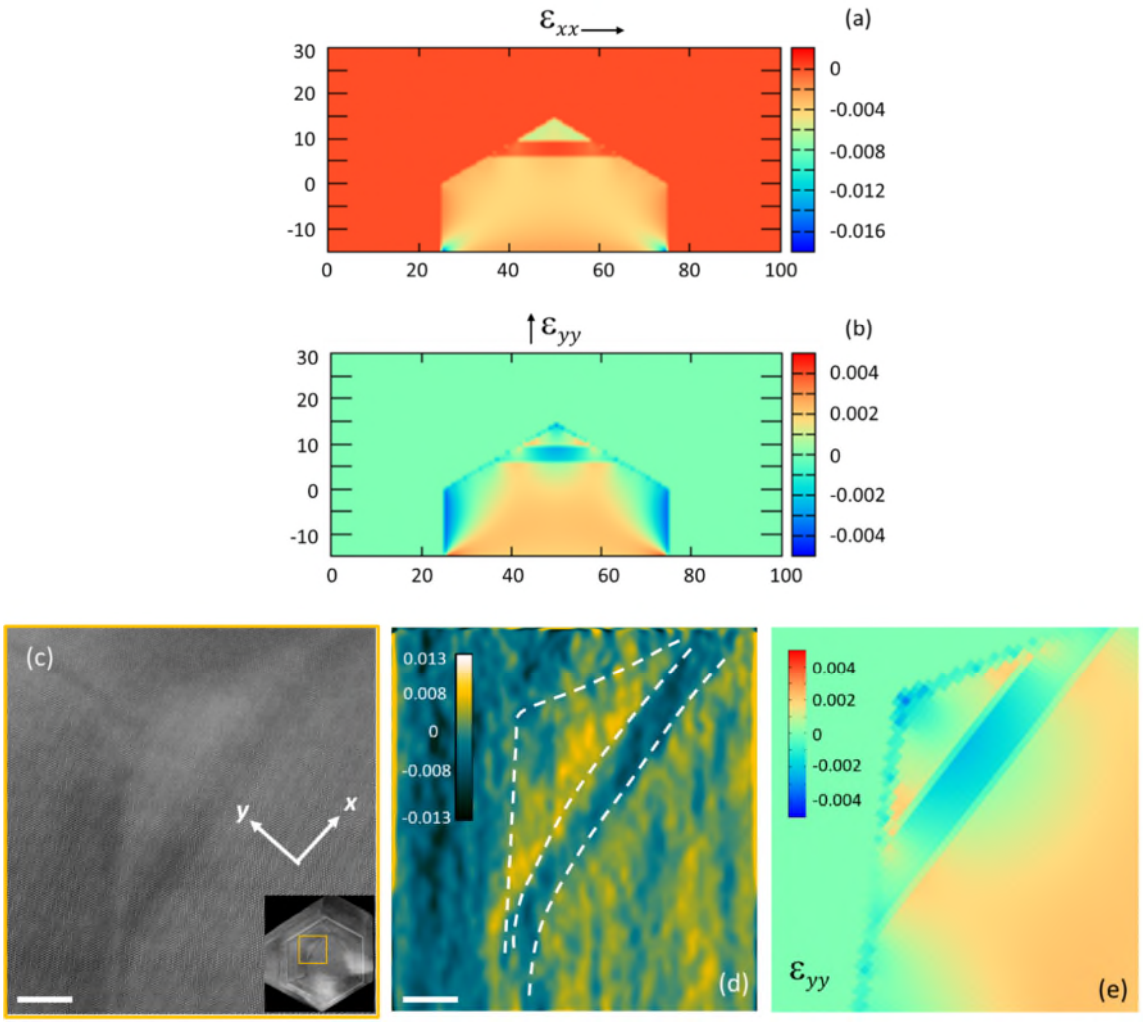

Figure S4. Simulated[5] 2-dimensional strain distribution in the (a) x and (b) y directions for a triangular region with parameter values equal to the average of the two shown in Figure 2 (c), that have been used for the simulation of the electronic band structure in Figures 3 (b), (c) and (d). (c) A higher magnification ADF STEM image of a wire from the cross section shown in Figure 2 (b) as marked by the yellow square in the inset. (d) Strain map of (c) in the y direction. Dashed lines show the region of the triangular wire obtained from (c) as a guide to the eye. (e) Simulated and scaled strain map obtained for the parameter values experimentally measured for the wire shown in (c) and (d). Scale bars are 5 nm.

Figure 4S (d) and (e) compares the same regions from an experimentally obtained strain map and a simulated one with the same parameter values. The difference in absolute values of the strain could be due to reasons such as relaxation of the thin TEM section towards natural lattice parameters in (d) compared to the constrained material in the simulation (e) and scanner distortions. However, it could be seen that the general strain distribution of the region is comparable, while some of the subtle features seen in the simulation are indistinguishable or lacking in the experimentally obtained map, possibly due to the same reasons as above.

Section S5: Types of optical behaviour expected from the axial wires formed at the edges of the GaAsP nanowire cores

Considering the interplay between the composition, strain and size (quantum confinement), the axial wires can be classified into four types according to their expected optical behaviour.

Type 1: P composition in the wire is lower than that of the core and the combination of compressive strain of the wire and quantum confinement is not sufficient to push the lowest confined state above the bandgap of the core. The electrons and holes are confined in the wire region, as this gives the lowest energy states of the system, allowing them to behave like QWRs.

Type 2: P composition of the wire is lower than that of the core, but the combination of the compressive strain of the wire (from the P rich band and GaAsP shell) and the quantum confinement is sufficient to increase the energy of the lowest confined states in the wire above those of the core. The example nanowire discussed in Figures 2 (c) and 3 (b) in the main manuscript falls into this category. Here, even though the wire region initially has the lowest P composition the compressive strain exerted on the wire increases the band gap of the wire region almost to the same value as that of the strained core, as shown in Figure 3 (b) in the main manuscript. The effects of quantum confinement further elevate the energy of the confined states above the band gap of the core. As a result, the nanowire core encompasses the lowest energy states. However, as shown in Figure 3 (b) and by probability densities for the lowest and highest electrons and hole states pertaining to the wire region in Figure 3 (c) and (d) in the main manuscript, the wire is still able to localise higher energy electron and hole states. The lowest electron and highest hole levels confined within the QWR lie 28 and 10 meV above and below that of the respective core states. This is similar to the behaviour seen for self-assembled QDs in the GaAs-AlGaAs material system, where the lowest energy continuum states are associated with the GaAs layer [6].

Type 3: The P composition of the wire is higher than that of the core and its band gap is further increased by the compressive strain exerted by the GaAsP shell and P rich band. The confinement will further elevate the energy of the confined QWR states. Yet, similar to type 2, it is still able to localise electron and hole states.

Type 4: This is similar to type 3, but no confinement of higher energy QWR-like states is observed within the number of electron and hole levels computed. This occurs when the effect of the P rich band becomes weak, either due to its effective band gap decreasing due to the tensile strain exerted by the core and the sufficiently large wire, and/or when the difference in composition between the wire and the P rich band becomes too low.

Therefore, in summary, it could be seen that three types of wires can behave as optically active QWRs with most having confined states that are higher in energy than that of the nanowire core.

Section S6: Single band effective mass simulations of the QD structures formed by the consecutive twinning of the nanowire

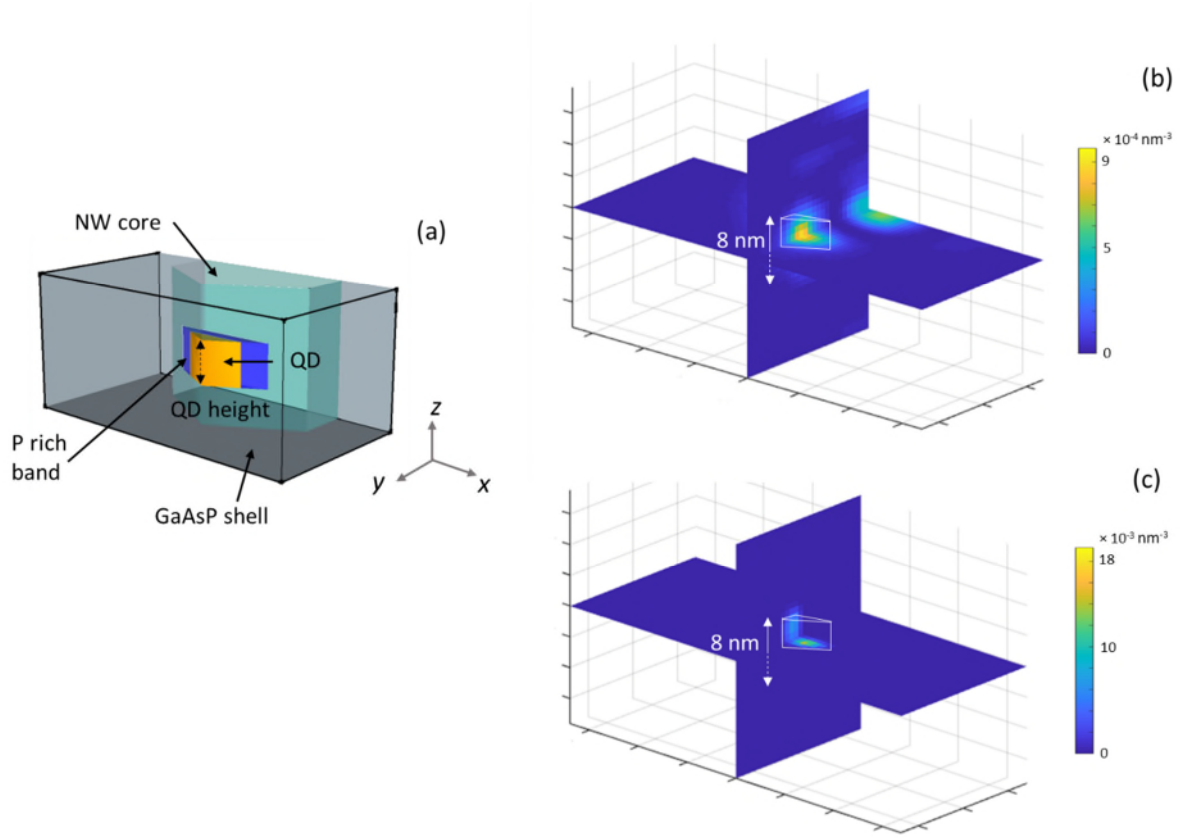

Figure S5. (a) A schematic of the simulated QD structure, formed by sandwiching a thin segment with similar cross-section to that in Figure 3 (a) between the nanowire core and shell slices that do not contain QWRs. (b) and (c) Probability densities of the lowest electron and highest hole states that are confined to an 8 nm high QD, with a parameter set similar to that of the QWR simulated in Figure 3 of the main manuscript, respectively. The white frame indicates the QD region for clarity.

Section S7: Proposed growth mechanism of the QWRs

Although a hexagonal cross-sectional shape is more common in wurtzite (WZ) and most zincblende (ZB) nanowire cores, truncated triangular, nonagonal and Reuleaux triangular cross sectional shapes have also been observed in the cores of ZB nanowires due to the asymmetry of the {112} facets (or their constituent {111} and {113}) facets), arising from the two polarities[3, 7, 8]. A similar observation is made here, with the nanowire core marked in Figure S6 (a) exhibiting a shape that is closer to that of a nonagon with partly formed {110} facets. The P rich band appears to have been formed during the initial stages of the Ga particle consumption step, when the Ga source is completely cut off and the P and As fluxes reduced. Similar bands have been found to form around the core in other nanowire growths, where particle consumption step was performed as shown in Figure S6 (b). The growth is presumed to have taken place using the residual Ga left in the chamber, incorporating P that is preferentially segregated on the ZB surfaces. The preferential segregation of P could be a result of the different segregation energies of P and As on the ZB surfaces under the growth conditions.[9]

The P rich band seen in the current growth, which is in contrast to the P rich ring in the {110} faceted core of a hexagonal shape, is a result of the much higher growth rate on the {112} B facets compared to the {110} facets[10]. In some nanowires, this P rich growth has been sufficient to complete the {110} faceted hexagonal shape, resulting in P rich triangles rather than bands, as shown in Figure S6 (c). Also, in some other nanowires, a combination of QWRs and P rich triangles are seen as a result of the unequal sizes of the initial {112} B facets. The continued particle consumption step could have an annealing effect on the parasitic island growth[11] that has taken place on the substrate during nanowire core growth, decomposing them. This decomposed material can redeposit on the preferential {112}B facets in a self-limiting manner[10, 12] forming the triangular regions and hence completing the {110} faceted hexagonal shape. The subsequent intentional GaAsP shell has a higher P composition than the triangular regions, making the latter relatively As rich QWRs that are surrounded by P rich regions.

The relatively large size and composition variation observed in these self-formed QWRs can be attributed to the random positioning of the nanowires on the substrate and variation in nanowire core sizes that result from variations in self-formed Ga droplet sizes [11, 13-15]. Controlling the uniformity of these structures is paramount for their usability in future applications. Growth on patterned substrates could greatly equalise composition variations arising from the presence of randomly positioned neighbouring nanowires and variation in size in the initial droplets [13, 15, 16].

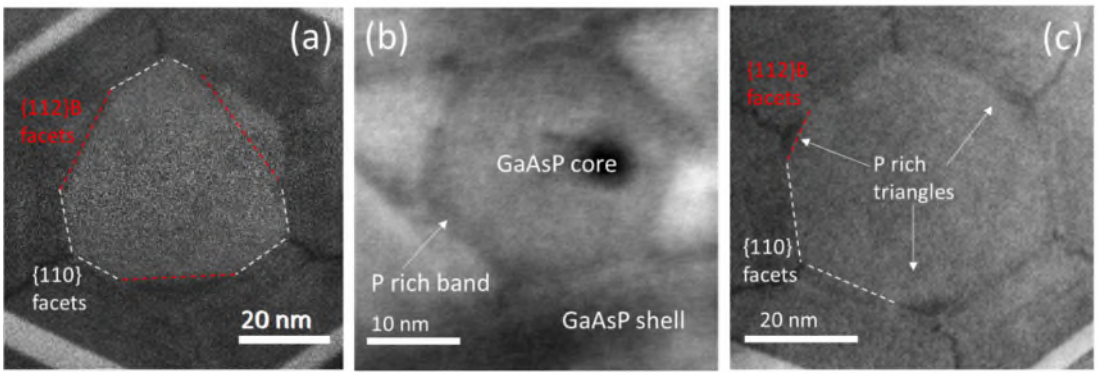

Figure S6. ADF images of (a) a nanowire cross-section from the discussed sample, showing the nonagon shaped (six {110} facets and three {112} B facets) GaAsP core within the P rich bands. (b) a nanowire cross-section from a different GaAsP-GaAsP core shell sample which also included a Ga particle consumption step. Here, the GaAsP core is hexagonal. However, a P rich band is visible at the core-shell interface in dark contrast. The dark spot visible closer to the centre of the core is due to beam damage caused during analysis. (c) a nanowire cross-section from the main discussed sample, where P rich triangular regions, instead of bands have formed.

References:

1. Fonseka, H. A. Growth and Characterisation of InP Nanowires and Nanowire-Based Heterostructures for Future Optoelectronic Device Applications. The Australian National University, 2015.
2. Sanchez, A. M.; Zhang, Y.; Tait, E. W.; Hine, N. D. M.; Liu, H.; Beanland, R. Nonradiative Step Facets in Semiconductor Nanowires. *Nano Letters* 2017, 17, 2454-2459.
3. Jiang, N.; Wong-Leung, J.; Joyce, H. J.; Gao, Q.; Tan, H. H.; Jagadish, C. Understanding the True Shape of Au-Catalyzed GaAs Nanowires. *Nano Letters* 2014, 14, 5865-5872.
4. Zheng, C.; Wong-Leung, J.; Gao, Q.; Tan, H. H.; Jagadish, C.; Etheridge, J. Polarity-Driven 3-Fold Symmetry of GaAs/AlGaAs Core Multishell Nanowires. *Nano Letters* 2013, 13, 3742-3748.
5. Birner, S.; Zibold, T.; Andlauer, T.; Kubis, T.; Sabathil, M.; Trellakis, A.; Vogl, P. nextnano: General Purpose 3-D Simulations. *IEEE Transactions on Electron Devices* 2007, 54, 2137-2142.
6. Heiss, M.; Fontana, Y.; Gustafsson, A.; Wüst, G.; Magen, C.; O'Regan, D. D.; Luo, J. W.; Ketterer, B.; Conesa-Boj, S.; Kuhlmann, A. V.; Houel, J.; Russo-Averchi, E.; Morante, J. R.; Cantoni, M.; Marzari, N.; Arbiol, J.; Zunger, A.; Warburton, R. J.; Fontcuberta i Morral, A. Self-assembled quantum dots in a nanowire system for quantum photonics. *Nat Mater* 2013, 12, 439-444.
7. Zou, J.; Paladugu, M.; Wang, H.; Auchterlonie, G. J.; Guo, Y.-N.; Kim, Y.; Gao, Q.; Joyce, H. J.; Tan, H. H.; Jagadish, C. Growth Mechanism of Truncated Triangular III–V Nanowires. *Small* 2007, 3, 389-393.
8. Verheijen, M. A.; Algra, R. E.; Borgström, M. T.; Immink, G.; Sourty, E.; van Enckevort, W. J. P.; Vlieg, E.; Bakkers, E. P. A. M. Three-Dimensional Morphology of GaP−GaAs Nanowires Revealed by Transmission Electron Microscopy Tomography. *Nano Letters* 2007, 7, 3051-3055.
9. Galicka, M.; Buczko, R.; Kacman, P. Segregation of Impurities in GaAs and InAs Nanowires. *The Journal of Physical Chemistry C* 2013, 117, 20361-20370.
10. Zhang, Q.; Aqua, J.-N.; Voorhees, P. W.; Davis, S. H. Mechanisms of morphological evolution on faceted core–shell nanowire surfaces. *Journal of the Mechanics and Physics of Solids* 2016, 91, 73-93.
11. Zhang, Y.; Sanchez, A. M.; Sun, Y.; Wu, J.; Aagesen, M.; Huo, S.; Kim, D.; Jurczak, P.; Xu, X.; Liu, H. Influence of Droplet Size on the Growth of Self-Catalyzed Ternary GaAsP Nanowires. *Nano Letters* 2016, 16, 1237-1243.
12. Biasiol, G.; Gustafsson, A.; Leifer, K.; Kapon, E. Mechanisms of self-ordering in nonplanar epitaxy of semiconductor nanostructures. *Physical Review B* 2002, 65, 205306.
13. Borgstrom, M. T.; Immink, G.; Ketelaars, B.; Algra, R.; Bakkers, E. P. A. M. Synergetic nanowire growth. *Nature Nanotechnology* 2007, 2, 541-544.

14. Kim, Y.; Joyce, H. J.; Gao, Q.; Tan, H. H.; Jagadish, C.; Paladugu, M.; Zou, J.; Suvorova, A. A. Influence of Nanowire Density on the Shape and Optical Properties of Ternary InGaAs Nanowires. *Nano Letters* 2006, 6, 599-604.

15. Oehler, F.; Cattoni, A.; Scaccabarozzi, A.; Patriarche, G.; Glas, F.; Harmand, J.-C. Measuring and Modeling the Growth Dynamics of Self-Catalyzed GaP Nanowire Arrays. *Nano Letters* 2018, 18, 701-708.

16. Zhang, Y.; Wu, J.; Aagesen, M.; Holm, J.; Hatch, S.; Tang, M.; Huo, S.; Liu, H. Self-Catalyzed Ternary Core–Shell GaAsP Nanowire Arrays Grown on Patterned Si Substrates by Molecular Beam Epitaxy. *Nano Letters* 2014, 14, 4542-4547.